THERMOMETRIC STUDY OF FIELD EMISSION IN A 1.3 GHZ SUPERCONDUCTING CAVITY

M. Pekeler[1], T. Fuljahn[1], P. Schmüser[1],
H. Padamsee[2], M. Champion[3], C. Crawford[3],
J. Graber[3], A. Matheisen[3], W.-D. Möller[3], D. Proch[3]

[1]II. Institut für Experimentalphysik der Universität Hamburg,
Notkestr. 85, 22603 Hamburg, Germany
[2]Laboratory of Nuclear Studies, Cornell University,
Ithaca, NY 14853-5001, USA
[3]DESY, 22603 Hamburg, Germany

Abstract

A 768-thermometer temperature mapping system with 40 ms total readout time was used for field emission studies on a single-cell 1.3 GHz niobium cavity, immersed in superfluid helium. Any significant change in the excitation function $Q_0(E_{acc})$ of the cavity (quality factor as function of accelerating field) could be associated with a modification in the temperature map. The energy deposition by field-emitted electrons was studied as a function of position on the cavity surface. The removal of field emitters by high power processing (HPP) was clearly visible on the temperature map. HPP improved the attainable gradient but in several cases reduced the low-field Q_0 of the cavity, probably due to surface contamination by material evaporated from the processed emitter.

1 Introduction

The TESLA design for a linear electron-positron collider in the 500 GeV to 1 TeV centre-of-mass energy regime is based on 9-cell 1.3 GHz superconducting niobium cavities with an accelerating field of at least 25 MV/m. This value, although considerably lower than the theoretical maximum of about 50 MV/m, is more than a factor of 2 above present-day standards [1]. The main limitations are due to thermal breakdown and field emission of electrons from the inner surface. A temperature mapping system is well suited to localize hot spots on the inner cavity surface and can be utilized to study the properties of field emitters and the effect of high power processing.

2 Experimental setup

The experiments were performed on a single-cell cavity with slightly elliptic cross section, built at Cornell University. Niobium with an initial residual resistivity ratio $RRR = 250$ was used and the cavity was heat-treated at 1400° C with titanium gettering to raise the RRR to 350. A surface layer of about 100 μm was removed by chemical etching. The cavity reached an accelerating gradient of 26 MV/m at Cornell. Prior to the RF tests at DESY, the inner surface was etched (15 μm), rinsed with de-ionized water and finally cleaned by high pressure water rinsing. The cavity was dried in a class 10 clean room and then mounted in a vertical test stand. Small vacuum leaks at the input-coupler side required in the two tests described here replacement of Helicoflex seals. It was decided to proceed with the tests without removing possible contaminants due to the leaks. The temperature maps indeed revealed some particle contamination of the cavity surface which, however, turned out useful for exploiting the capabilities of the diagnostic system.

In the vertical dewar the RF power is guided into the cavity through a rectangular 1.3 GHz waveguide with a door-knob like transition to a coaxial input coupler. For continuous wave (CW) operation a 250 W solid state amplifier is used while high power processing (HPP) is performed with a 4 MW klystron with a maximum pulse length of 2 ms. The highest power the cavity was exposed to during HPP was 700 kW. The cavity is bath-cooled with superfluid helium of 1.5 K.

A temperature mapping system was built at Cornell University and DESY, following a design for 1.5 GHz cavities [2]. It consists out of 768 spring-loaded thermometers (see Fig. 1a) whose basic component is a 100 Ω Allen-Bradley carbon resistor (room temperature value). In liquid helium the resistance is strongly temperature dependent, ranging from 1000 Ω at 4 K to about 15 kΩ at 1.5 K.

To improve the thermal contact, Apiezon N grease is used which effectively prevents superfluid helium from penetrating the gap between thermometer and cavity surface. The thermometers are mounted on printed circuit boards of two different types (see Fig. 1b) to achieve optimum coverage of the cavity surface including the beam tube sections. Each board covers a meridian of the cavity. A cross section of the cavity is shown in Fig. 2a. The azimuthal angle between adjacent boards is 7.5°; there are 24 boards with 19 thermometers each and 24 boards with 13 thermometers. The resistors are fed with a constant current of 10 μA and the voltages are guided out of the cryostat via parallel cables and connectors at the vacuum flange to type NI-SCXI-1100 multiplexers and a NI-MIO-16XL analog to digital converter. The thermometers are read out sequentially, the total readout time being 40 ms.

Data collection and analysis is performed using LabVIEW on a Macintosh Quadra 950 computer. During cooldown from 4.2 K to 1.5 K all thermometers are individually calibrated at 0.1 K intervals against the temperature derived from the helium vapour pressure. The helium bath temperature T as

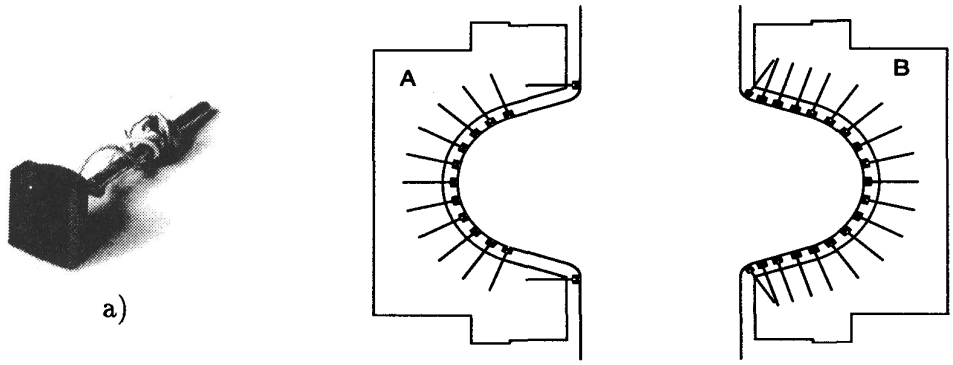

Figure 1: a) Thermometer of the temprature mapping system. b) Schematic of the two different thermometer boards.

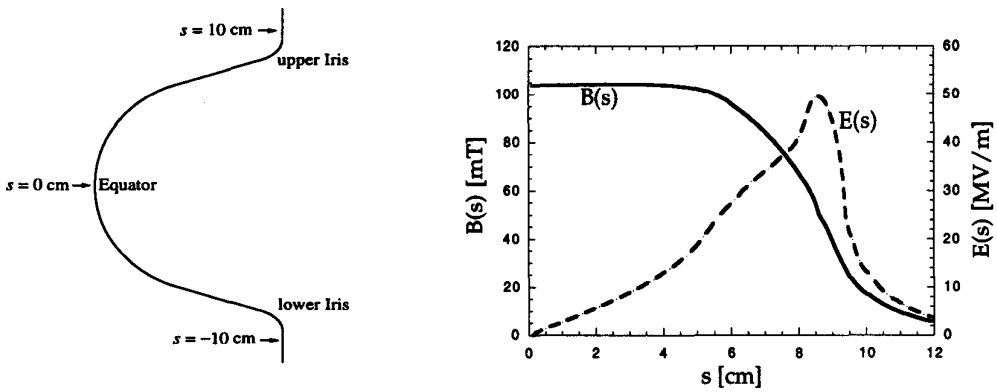

Figure 2: a) Definition of the coordinate s. b) Local magnetic field $B(s)$ and local electric field $E(s)$ as a function of the coordinate s. The values are calculated for an accelerating gradient of $E_{\mathrm{acc}} = 25$ MV/m.

a function of resistance R is parametrized in the form

$$\frac{1}{T} = \sum_{i=0}^{4} a_i (\ln R)^i \,. \tag{1}$$

The resolution is in the order of 2 mK.

To create a temperature map of the cavity surface, readings with and without RF field in the cavity are made and then subtracted. Besides temperature maps of the entire cavity, selected boards can be read out at higher repetition rate. This permits the study of transient heating at field-emitting locations.

The response of the thermometers to heating of the inner cavity surface is determined experimentally by measurements at low fields. As long as no 'hot spot' is present in the cavity, the dissipated power P_{diss} per unit area, which can be derived from the incident and reflected RF power, is deposited rather uniformly over the cavity surface. The average temperature rise $\langle \Delta T \rangle$

of all thermometers is found to increase linearly with $P_{\rm diss}$. From these data we have determined the average thermometer sensitivity:

$$\eta_{\rm th} = \langle \Delta T \rangle / P_{\rm diss} = 2 \cdot 10^{-4}\ {\rm K/(W/m^2)} \qquad (2)$$

which should be accurate to within a factor of 2 (a more precise calibration appears hopeless because the heat transfer coefficient between cavity surface, Apiezon grease and carbon resistor is extremely sensitive to small amounts of superfluid helium penetrating the gap).

3 Field limitations in superconducting cavities

3.1 Thermal Breakdown

The high-frequency magnetic field induces eddy currents of the normal (non-superconducting) electrons in a thin surface layer. A thermal breakdown or quench starts usually in a region of increased surface resistance, either a normal-conducting zone, a defect or a foreign particle. If more heat is generated than can be conducted away through the bulk material into the surrounding superfluid helium bath, the normal area starts to grow, thereby producing more and more heat, until the whole stored energy of the cavity is dissipated in the warm region. A high thermal conductivity of the wall material is essential for avoiding thermal breakdown at low field levels.

The power density generated by the eddy currents is proportional to the square of the local magnetic field. The strength of the local magnetic field $B(s)$ along a meridian is plotted in Fig. 2b; $B(s)$ has its peak value B_p at the equator at $s = 0$ and drops rather slowly towards the iris.

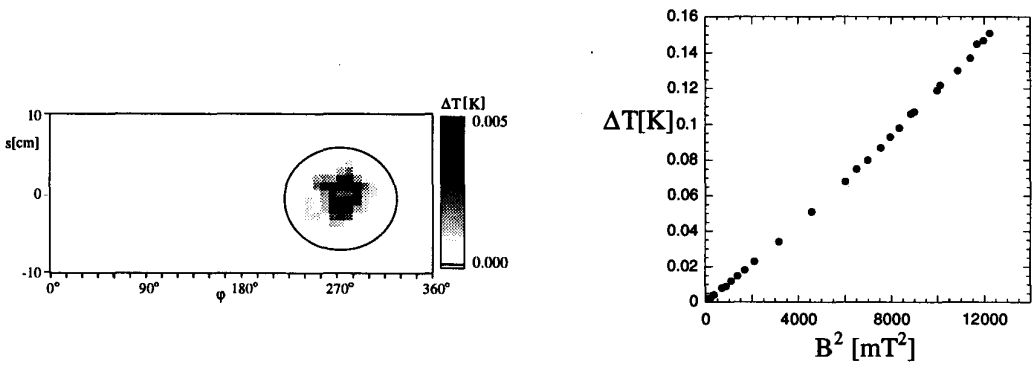

Figure 3: a) Unfolded temperature map of the cavity at an accelerating field of 2.5 MV/m. Circled is an area with high surface Resistance. b) Heating ΔT of the hottest thermometer in dependence of the square of the local magnetic field B.

An example of eddy-current heating in an area of increased surface resistance is shown in Fig. 3. The temperature map (Fig. 3a) reveals a warmer

zone near the equator at an azimuthal angle of 270°. The temperature rise in the area is plotted in Fig. 3b as a function of B^2, where B is the local field. The parabolic law is very well obeyed.

3.2 Field Emission

Field emission of electrons via the quantum-mechanical tunnel effect depends exponentially on the local electric field $E(s)$ which may be strongly enhanced at small tips or sharp edges. Assuming a smooth cavity surface the local electric field has been calculated using the finite-element code SUPERFISH. In Fig. 2b $E(s)$ is plotted as a function of the coordinate s along a meridian; the numbers refer to an accelerating field on the cavity axis of $E_{\mathrm{acc}} = 25$ MV/m. The local electric field vanishes at the equator and has a pronounced peak near the iris with $E_{\mathrm{peak}} = 1.98 \cdot E_{\mathrm{acc}}$. Hence field emission should predominantly occur in this region. The electron current density is given by the Fowler-Nordheim equation

$$j_{\mathrm{FE}} = c_1 E^{2.5} \exp(-\frac{c_2}{\beta E}). \tag{3}$$

Here c_1 and c_2 are constants and $E \equiv E(s)$ denotes the computed local field (assuming a smooth surface). In comparison with field emission from a planar metal surface in a d.c. electric field there are two modifications:

(1) A so-called *field enhancement factor* β is introduced as an adjustable parameter to account for the fact that field emission usually proceeds at small tips or sharp edges where the field is strongly enhanced; typical values are $\beta = 100 - 200$.

(2) Field emission in RF fields is characterized by a factor $E^{2.5}$ in front of the exponential instead of the well-known E^2 factor in d.c. fields.

The electrons are accelerated in the RF electric field and extract energy from the cavity, thereby reducing its quality factor. A question of great concern is where they impinge on the wall and deposit their kinetic energy in the form of heat. Computed trajectories are plotted in Fig. 4a for an emitter near the iris. Since the electric field has no azimuthal component, the trajectories emerging from a point source are confined to the plane defined by the meridian on which the emitting site is located and the centre axis of the cavity. The exponential factor in Eq. (3) has the consequence that field emission occurs only in a limited interval of the RF phase (say $(90 \pm 25)°$ for a sinosoidal time dependence of the surface electric field $E(t) = E_0 \sin \omega t$). This has a significant impact on the trajectory pattern.

In Fig. 4a the trajectories of electrons leaving the emitter in a $(90 \pm 25)°$ interval of the RF phase are shown. The majority hit the cavity wall in the same hemisphere where the emitter is located. The computed energy deposition along the meridian, translated into a temperature rise ΔT of the thermometers by using the sensitivity factor η_{th}, is depicted in Fig. 4b. One can see that the lion's share of the energy is deposited in the immediate vicinity of the emitter. This observation is verified by experiment. A pronounced field emitter was found at $s = -8.73$ cm, $\varphi = 160°$, see Fig. 4c. The measured ΔT distribution (Fig. 4d) resembles closely the simulated distribution.

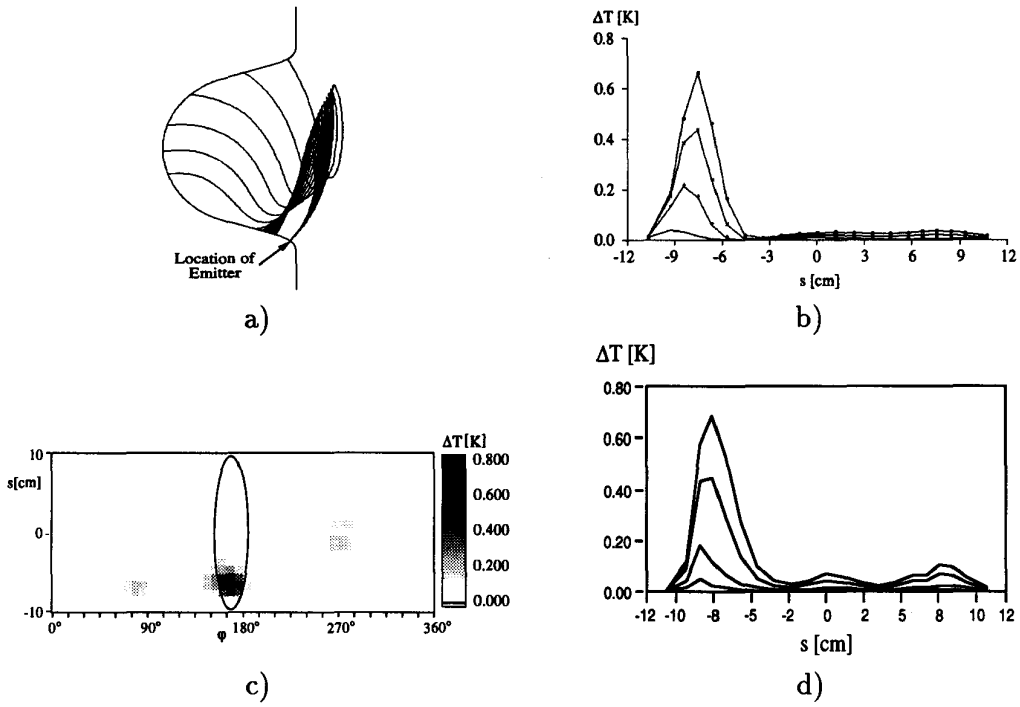

Figure 4: a) Computed trajectories from electrons emitting out of a field emitter at a phases $(90 \pm 25)°$ of the RF field. b) Calculated heating of the outer surface for the electrons following the trajectories shown in a) for 4 different electric field levels. c) Tamperature map with a candidate for field emission. d) Measured temperature distribution of the field emitter for the 4 electric field levels.

3.3 Thermionic Emission

Foreign particles sticking to the inner surface with poor thermal contact to the bulk material can be eddy-current heated to temperatures where thermionic electron emission takes place. The hot particle emits a current density given by the Richardson equation

$$j_{\mathrm{TE}} = c_3 \, T^2 \exp(-\frac{\Phi}{k_{\mathrm{B}} T}) \, . \tag{4}$$

Here c_3 is a constant, Φ is the work function of the emitting particle and k_B the Boltzmann constant. The temperature T of the emitter increases with the square of the local magnetic field $B(s)$ which in turn is proportional to the magnitude E_0 of the local electric field. Introducing new constants c_4, c_5 the thermionic current density can also be written as

$$j_{\mathrm{TE}} = c_4 \, E_0^4 \exp(-\frac{c_5}{E_0^2}) \, . \tag{5}$$

The trajectory computation for thermally emitted electrons differs from the above case in that all RF phases during the positive half wave are now equally admissible. The trajectory pattern (Fig. 5a) has indeed a very different appearance: the majority of thermally emitted electrons hit the hemisphere

opposite to the emitter. The computed ΔT distribution is plotted in Fig. 5b. A candidate for a thermionic emitter is depicted in the temperature map in Fig. 5c ($s = -7.5$ cm, $\varphi = 340°$). The measured ΔT distribution (Fig. 5d) exhibits indeed the predicted peak in the opposite hemisphere but in addition there is a peak near the emitting site. The most obvious explanation is direct heating of the cavity surface by the hot particle. This effect is not included in the simulation of Fig. 5b.

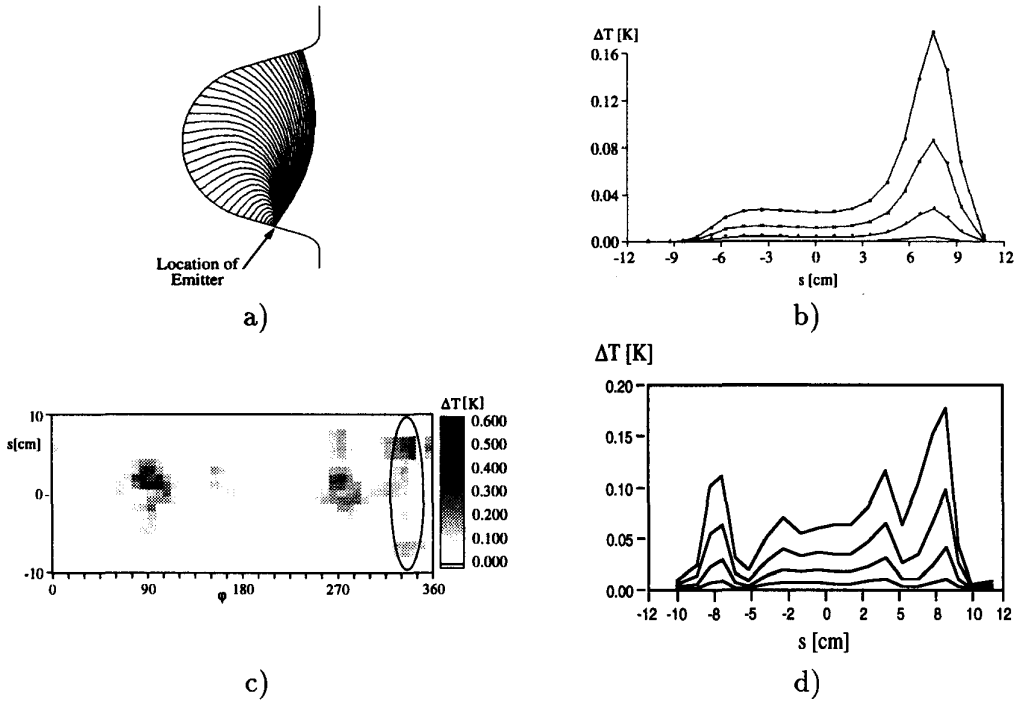

Figure 5: a) Trajectories for a thermionic emitter. All phases during the positive half wave are taken into account. b) Calculated temperature distribution on the outside of the cavity for this thermionic emitter. c) A candidate for thermionic emission. d) heating of the thermionic emitter in c) for different electric field levels.

3.4 Distinction between field and thermionic emitters

A standard method for determining the unknown field enhancement factor β consists in measuring the electron current from a field emitter as a function of the local field E_0 and plotting the logarithm of $j_{FE}/E_0^{2.5}$ against $1/E_0$. This is called a 'Fowler-Nordheim plot'. In the present experiment we have determined the temperature rise of the thermometers which is proportional to the electron current density j_{FE}, multiplied with the kinetic energy gained by the electrons which grows linearly with E_0. For this reason we plot of $\ln(\langle\Delta T\rangle/E_0^{3.5})$ versus $1/E_0$. For the data of Fig. 5d the plot is shown in Fig. 6a. An almost linear relationship is observed from which one derives a field enhancement factor $\beta \approx 190$.

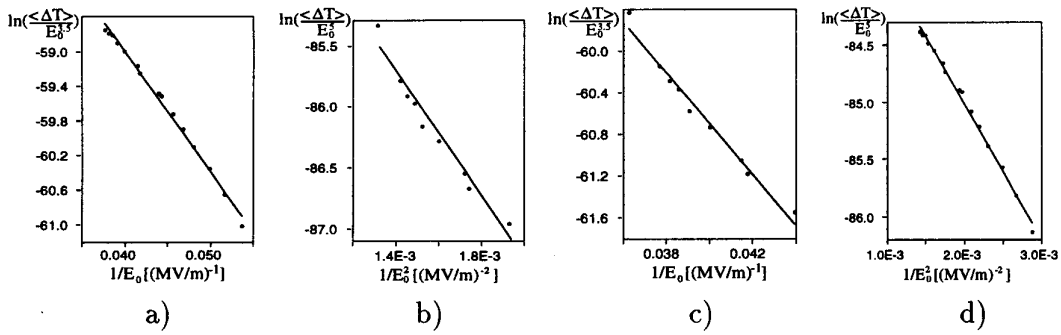

Figure 6: a) Fowler-Nordheim plot for the field emitter of Fig. 4. b) Richardson plot of the thermionic emitter shown in Fig. 5. c) 'Wrong' Fowler-Nordheim plot for the thermionic emitter. d) 'Wrong' Richardson plot for the field emitter.

For thermionic emission one should, according to Eq. (5), plot $\ln(\langle\Delta T\rangle/E_0^5)$ versus $1/E_0^2$ and use only the temperature data in the hemisphere opposite to the emitter since the energy deposited close to the emitting site is most likely due to direct heating. The resulting 'Richardson plot' is shown in Fig. 6b. Also here the data are described quite well.

In practice it is difficult to decide from the Fowler-Nordheim or the Richardson plot whether a measured temperature increase is caused by field or thermionic emission. In Figs. 6c, 6d we have purposely plotted the previous data in the wrong way, the field emitter is analyzed as a thermionic emitter and vice versa. Apparently these 'wrong' fits are not bad either. If two peaks are observed thermionic emission is the preferred interpretation.

There may be cases where both effects are contributing. For instance it is conceivable that a sharp tip starts field emission; with increasing field strength it is heated up until the tip melts and field emission stops but the site has become so hot that it continues to release electrons via thermionic emission.

3.5 Cures against emission sites

Absolute cleanliness during the various stages of cavity handling (heat treatment, chemical etching, water rinsing and assembly) is the prerequisite for good performance. With these measures the field emission threshold is usually pushed beyond $E_{\rm acc} \geq 10$ MV/m. High-pressure water rinsing reduces the emitter density. A technique for improving the performance of a cavity already installed in the cryostat is high power processing (HPP) [3][4][5]. The input coupler is moved further into the cavity beam pipe to get strong overcoupling and a fast rise time of the cavity field. Then RF pulses of high instantaneous power (several hundred kW for a single-cell cavity) are applied whose duration is so short ($\leq$ 1 ms) that a general thermal breakdown is avoided. The rapidly rising field causes strong electron emission at field emitters and heats the sites so violently that they melt or evaporate. After high power processing an emitter has usually disappeared and the cavity can be excited to higher fields in normal CW operation.

4 Evolution of the emission characteristics during RF tests

4.1 First test sequence

The initial excitation curve $Q_0(E_{acc})$ of the cavity in the first test sequence is presented in Fig. 7. The temperature maps corresponding to the labeled points in Fig. 7 are shown in Fig. 8.

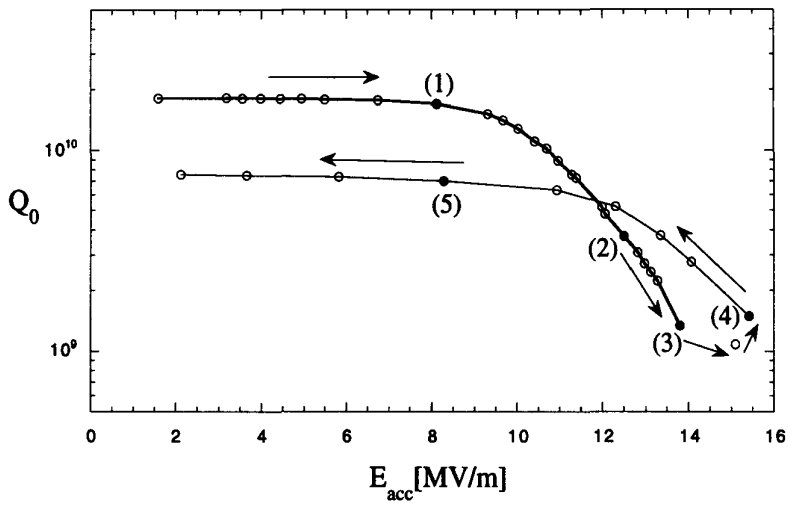

Figure 7: Q_0 versus E_{acc} behaviour of the cavity during the first test sequence directly after the first cooldown to 1.5 K.

Starting from a quality factor $Q_0 = 1.8 \cdot 10^{10}$ the curve stays flat up to 8 MV/m (point 1). Map 1 reveals an area of $\approx$ 15 cm^2 with an increased surface resistance which, from the measured dissipated energy, can be estimated to be in the order of 500 nΩ. The drop of Q_0 towards higher fields is associated with the appearance of a field emitter at the lower iris ($\varphi = 170°$) which is clearly visible in the second temperature map. Increasing the field to 14 MV/m opens another emitter (map 3). A small additional rise of the incident RF power leads to a discontinuous change in the excitation curve: in two steps point 4 is reached which has nearly the same Q_0 value as point 3 but at a higher field. The temperature map 4 reveals the origin of this improvement: the second emitter has disappeared. This is an example of 'low-power' processing (the cavity was powered with the 250 W amplifier in CW mode). Map 4 shows another remarkable feature: at the azimuthal position of the processed emitter an area of increased heat generation has been created near the equator. From the reduction in quality factor the surface resistance is estimated to be $\approx$ 600 nΩ. A possible explanation is that material evaporating from the emitter was deposited in this area and contaminated the surface. Returning to low field shows that a clear Q_0 degradation to $7 \cdot 10^9$ has taken place; basically the whole excitation curve $Q_0(E_{acc})$ has been moved down-

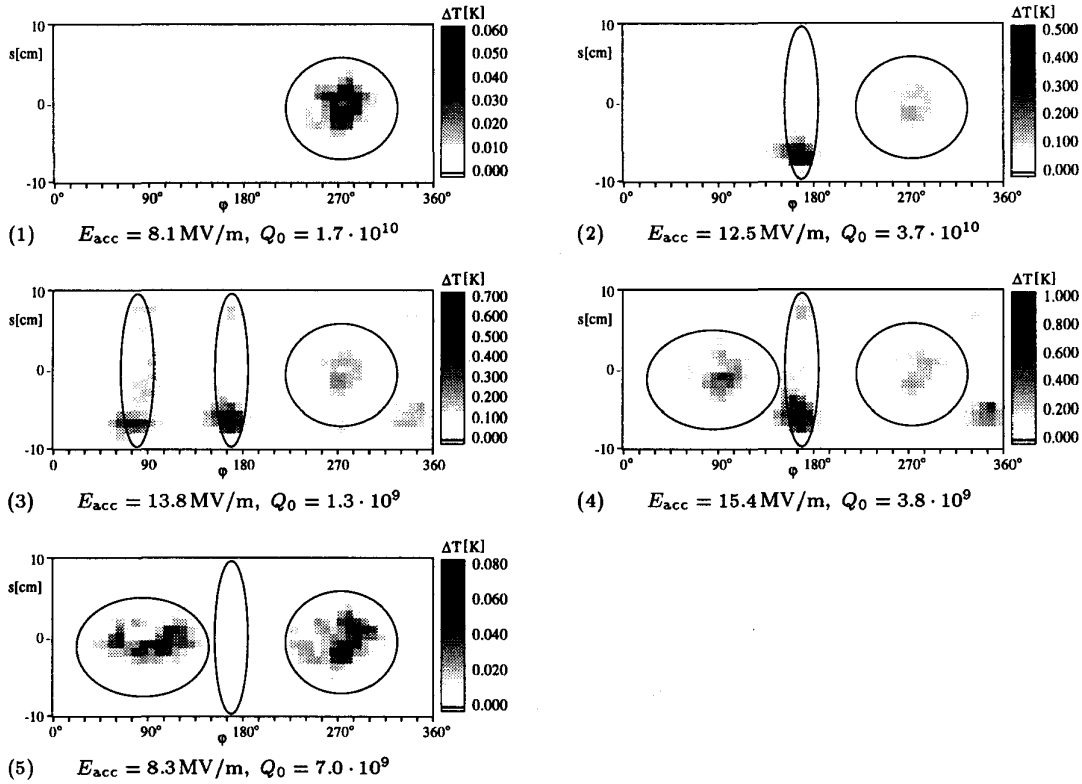

Figure 8: Temperature maps taken at the numbered points of the measurement in Fig. 7

wards but extends now to somewhat higher fields than before. The strong emitter was not affected by the available low-power RF field.

This measurement series shows that processing of emitters may be accompanied with a Q_0 degradation due to surface contamination.

Since the strong emitter and some other emitting sites could not be removed with an RF power of 250 W it was decided to apply high power processing. Owing to a superfluid-helium leak in the waveguide HPP had to be performed at 4.2 K. The peak power was 250 kW at a pulse length of 2 ms. In the subsequent low-power test in CW mode the top excitation curve in Fig. 9 was obtained which has two remarkable features: the original Q_0 has been completely recovered and the excitation curve stays flat up to 14 MV/m. The temperature maps 1 and 2 (Fig. 10) demonstrate that the strong emitter of the first test sequence has been eliminated. In addition the areas of increased surface resistance (map 5 in Fig. 8) have disappeared. (The reason may be surface heating in the HPP procedure accompanied with degassing).

With increasing field, $Q_0(E_{acc})$ follows a smooth excitation curve up to point 2 at 18.6 MV/m and $Q_0 = 4.4 \cdot 10^9$ where temperature map 2 reveals a hot spot near the equator at $\phi \approx 300°$. Just above this point a jump is observed leading to point 3 on the second $Q_0(E_{acc})$ curve; the much reduced performance is caused by the emitter shown in map 3.

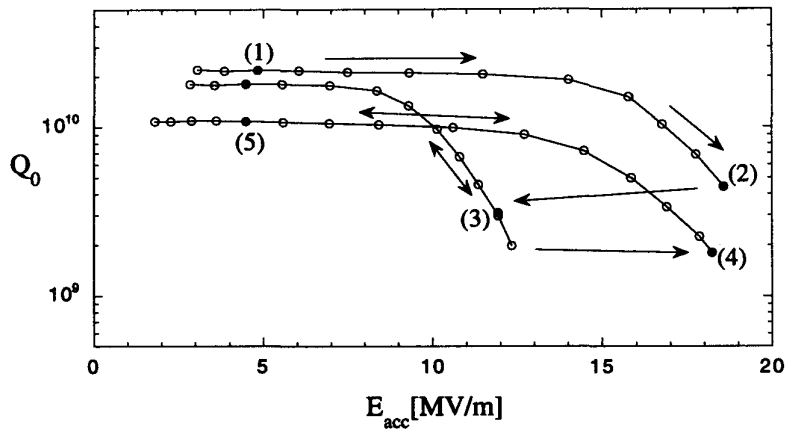

Figure 9: Q_0 versus E_{acc} behaviour of the cavity during the first test sequence after applying HPP, which was done at 4.2 K. Then the system was cooled down to 1.5 K again

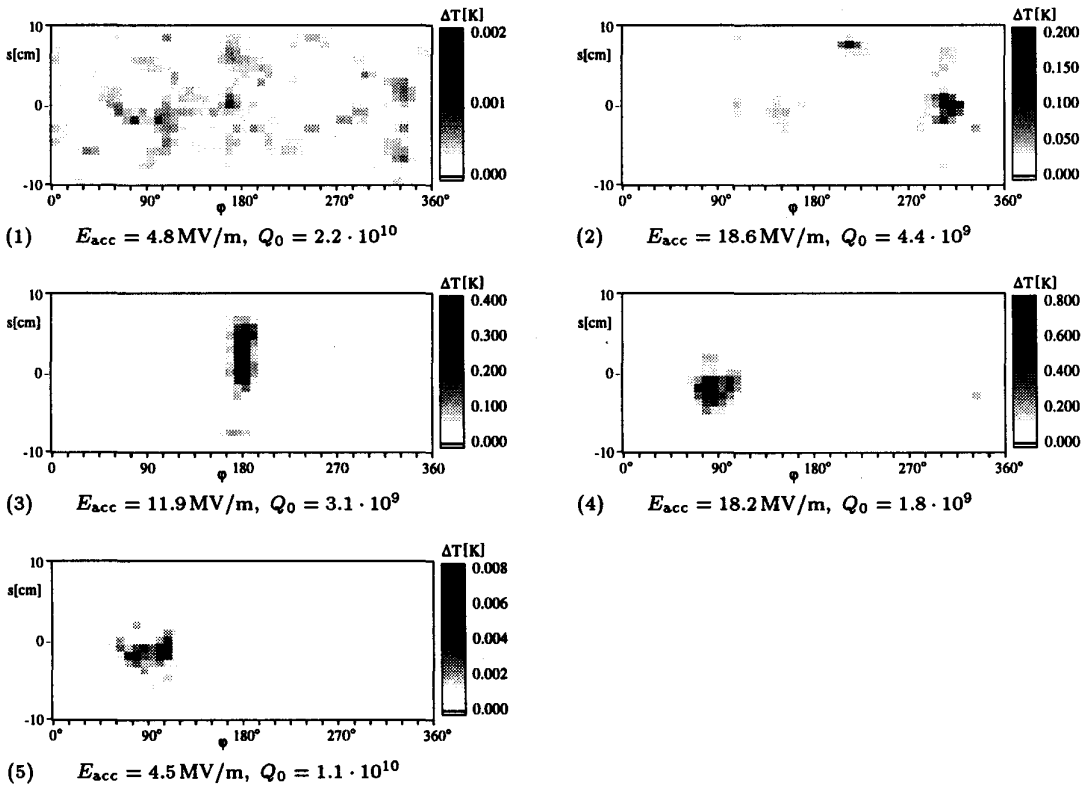

Figure 10: Temperature maps taken at the numbered points of the measurement in Fig. 9

The second $Q_0(E_{acc})$ curve can be traced out reversibly but going beyond point 3 leads to a genuine low-power processing event: there is a discontinuous transition to point 4 at almost constant Q_0 but with a significant increase in field. Temperature map 4 shows that the emitter seen in map 3 has been removed. Instead a large region of increased surface resistance is observed. The third excitation curve can again be traced out reversibly. At low field the quality factor is appreciably lower than the initial value. A region of increased surface resistance is seen also here (map 5) and explains the Q_0 degradation (compare map 1). This is another example that processing of an emitter may be accompanied with a reduction of the low-field quality factor. The most likely explanation is surface contamination by material evaporating from the emitter site during processing.

In addition to this test HPP was performed again at 4.2 K. This time 500 kW at 1 ms long pulses were supplied to the cavity. The quality factor at low field values was again recovered to $2.5 \cdot 10^{10}$, but after a processing event which took place at a field value of $E_{acc} = 21$ MV/m, the low field Q_0 was reduced to $9 \cdot 10^9$ and a region with high surface resistance created. The cavity now showed thermal breakdown at 20 MV/m, starting in the new region with higher surface resistance.

4.2 Second test sequence

After a new chemical etching of the inner surface (15 μm removal) a second test sequence was performed. The cavity started with a low-field Q_0 of $2.5 \cdot 10^{10}$ and reached 19.5 MV/m with low-power conditioning.

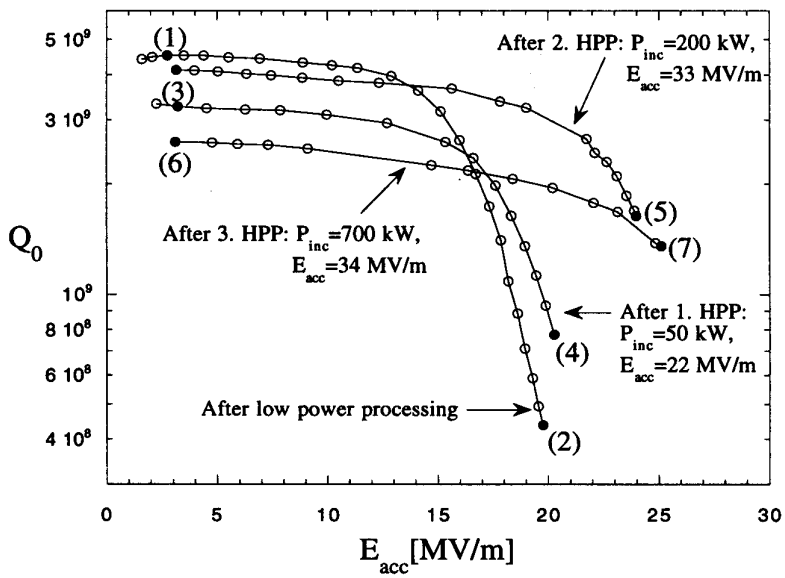

Figure 11: Q_0 versus E_{acc} measurement after HPP sessions during the second test sequence.

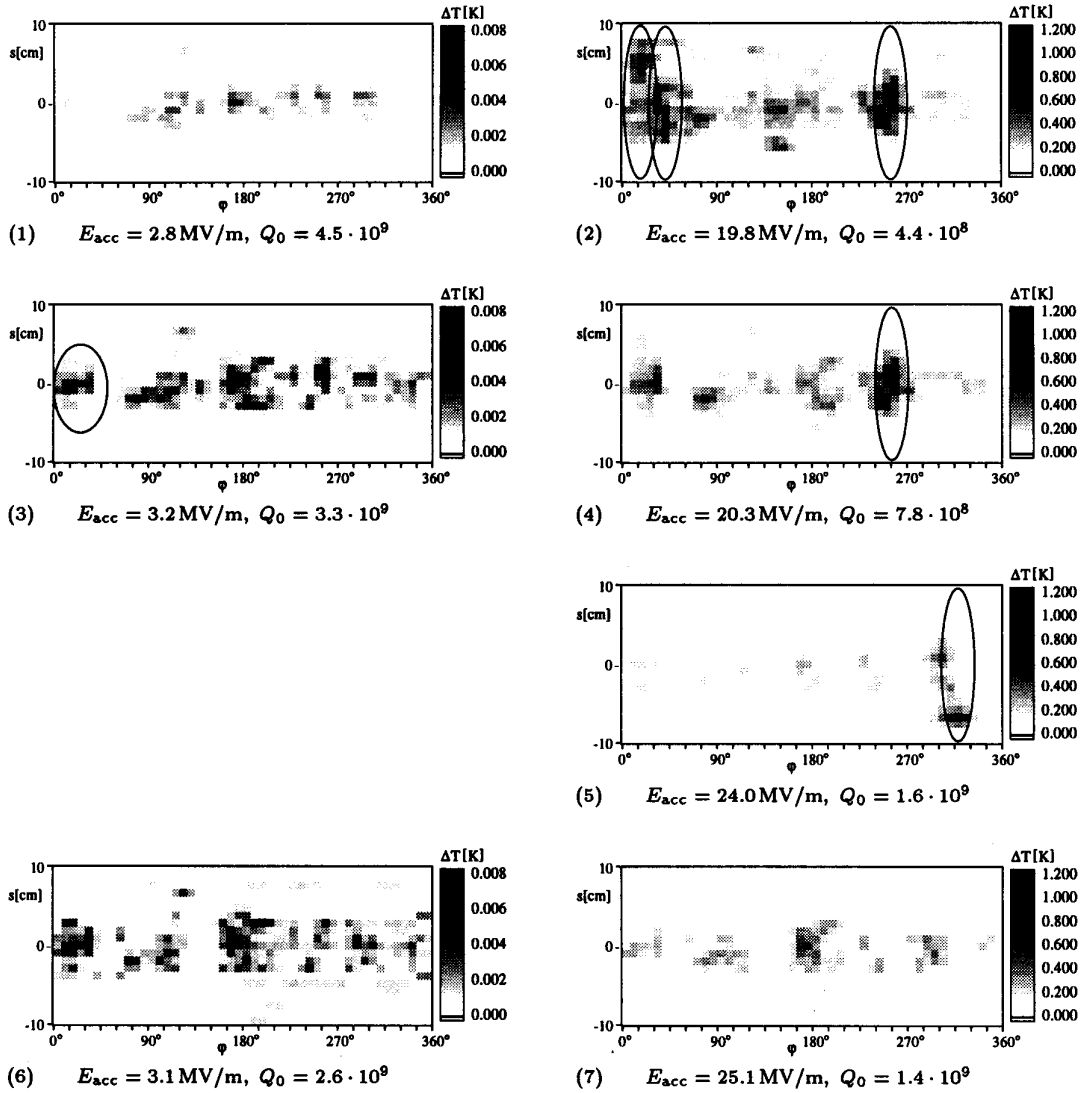

Figure 12: temperature maps taken during the measurement of Fig. 11.

The processing generated again regions with higher surface resistance which degraded the quality factor to $4.5 \cdot 10^9$ at low field (Fig. 11 and map 1, Fig. 12). At the highest fields three emitters were present (map 2 of Fig. 12).

Now HPP was carried out at 1.5 K. At an incident power of $P_{inc} = 50$ kW a processing event occured, characterized by a decay of the transmitted-power signal in less than 1 μs. The exitation curve measured in CW operation (Fig. 11) showed a further reduction in the low-field quality to a value $Q_0 = 3.3 \cdot 10^9$. Temperature map 3 shows a new region with high surface resistance. Map 4, taken at high field, proves that two emitters were destroyed during the processing event but one active emitter remained.

Raising the klystron power to 200 kW in the next HPP step resulted in a lot of processing events (more than 20). The first remarkable result of the following CW excitation curve was that this time HPP increased the low-field

quality factor $Q_0 = 4 \cdot 10^9$ at $E_{acc} = 3.1$ MV/m. Map 5 sows that the previous emitter, visible in map 4, was destroyed by HPP but a new emitter opened, limiting the field to $E_{acc} = 23$ MV/m.

A last HPP session was done with klystron power up to 700 kW at 250 μs pulse length, during which the cavity reached 34 MV/m. This reduced the low-field Q_0 to $2.6 \cdot 10^9$ (map 6). The highest attainable field was 25.1 MV/m, limited by thermal breakdown. No more emitters were visible now, see map 7. The exitation curve $Q_0(E_{acc})$ could be traced out reversibly now.

After this test sequence the whole system was warmed up to room temperature, pumped over the weekend and cooled back to 1.5 K. At the beginning the cavity had a quality factor of $Q_0 = 2.7 \cdot 10^{10}$ up tp a field level of 14.4 MV/m without indication of significant heating (less than 20 mK) in the temperature map. Trying to reach higher fields resulted in an erratic response of the cavity, not shown in Fig. 13. Finally a stable excitation curve was reached with a low-field $Q_0 = 4.7 \cdot 10^9$ (map 1 in Fig. 14) and a highest accelerating gradient of 17.4 MV/m. At this field level, the corresponding temperature map 2 shows a strong heating of almost the entire cavity surface.

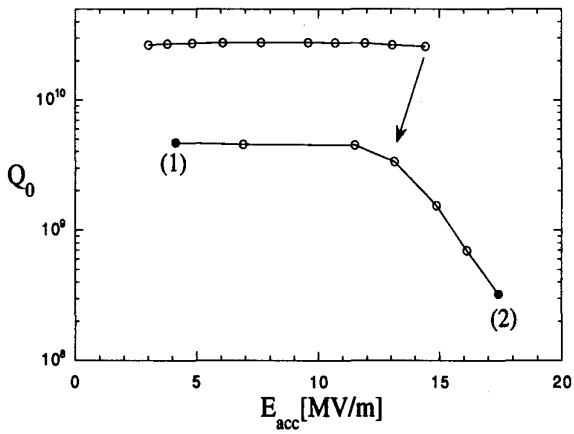

Figure 13: Q_0 versus E_{acc} measurement during the second test sequence after warming up the cavity to room temperature and then cool down again.

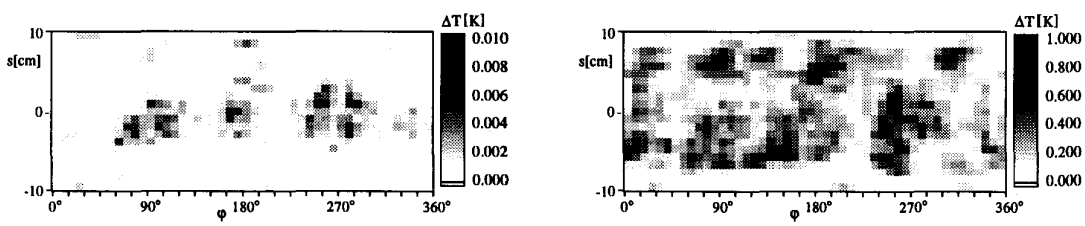

(1) $E_{acc} = 4.2$ MV/m, $Q_0 = 4.7 \cdot 10^9$ (2) $E_{acc} = 17.4$ MV/m, $Q_0 = 2.9 \cdot 10^8$

Figure 14: Temperature maps for the highlighted points of the measurement in Fig. 13

5 Conclusions

The tests described above were carried out on a single-cell cavity which contained a certain amount of contaminants due to vacuum leak problems. They are not representative for the performance that can be achieved under best clean room conditions. Rather these investigations illustrate the capabilities of a temperature mapping system covering almost the entire cavity surface and its use in investigating low- and high-power processing of emitters. In many cases regions with increased surface resistance were found as a consequence of HPP, indicating material evaporated from the processed emitter was deposited on the surface. Warming up effectively removed these lossy regions. Further studies are needed to determine the nature of the contaminants by residual gas analysis.

References

[1] W.-D. Möller, *Quest for high gradients*, this workshop.

[2] J. Knobloch, H. Muller and H. Padamsee, *Design of a High Speed, High Resolution, Thermometry System for 1.5 GHz Superconducting Radio Frequency Cavities*, internal Report SRF 940419-03, Cornell University, submitted to *Review of Scientific Instruments.*

[3] J. Graber *et al.*, *Proc. of the 1993 Particle Accelerator Conference, Washington, DC* (IEEE Cat. No. 3279-7,p. 886, 1993).

[4] J. Graber, *High power RF processing studies of 3 GHz Niobium superconducting accelerator cavities*, Dissertation, Cornell University, Ithaca, NY.

[5] C. Crawford *et al.*, *High Gradients in linear collider superconducting accelerator cavities by high pulsed power to surpress field emission, Particle Acceleratores*, 1995, Vol. 49, pp. 1-13.